optica

Discrete Anderson speckle

H. Esat Kondakci, Ayman F. Abouraddy, and Bahaa E. A. Saleh*

CREOL, The College of Optics & Photonics, University of Central Florida, Orlando, Florida 32816, USA

*Corresponding author: besaleh@creol.ucf.edu

Received 14 November 2014; revised 9 January 2015; accepted 9 January 2015 (Doc. ID 226790); published 26 February 2015

When a disordered array of coupled waveguides is illuminated with an extended coherent optical field, discrete speckle develops: partially coherent light with a granular intensity distribution on the lattice sites. The same paradigm applies to a variety of other settings in photonics, such as imperfectly coupled resonators or fibers with randomly coupled cores. Through numerical simulations and analytical modeling, we uncover a set of surprising features that characterize discrete speckle in one- and two-dimensional lattices known to exhibit transverse Anderson localization. First, the fingerprint of localization is embedded in the fluctuations of the discrete speckle and is revealed in the narrowing of the spatial coherence function. Second, the transverse coherence length (or speckle grain size) is frozen during propagation. Third, the axial coherence depth is independent of the axial position, thereby resulting in a coherence voxel of fixed volume independently of position. We take these unique features collectively to define a distinct regime that we call discrete Anderson speckle.

OCIS codes: (030.6600) Statistical optics; (030.1640) Coherence; (030.6140) Speckle; (290.4210) Multiple scattering.

http://dx.doi.org/10.1364/OPTICA.2.000201

1. INTRODUCTION

Speckle, the granular spatial intensity pattern imbued to a coherent optical field after traversing a disordered medium or reflecting from a rough surface, has been studied for decades extending back to the invention of the laser [1,2] and was known even earlier in radio waves [3,4]. It is a universal phenomenon associated with the interference of random waves. An archetypical arrangement is shown in Fig. 1(a), where a coherent wave traverses a thin phase screen and the random phase is converted into random intensity upon free-space propagation, which we refer to hereon as *conventional speckle*. Indeed, the propagation of light in random media or scattering from rough surfaces is critical to practical applications in bioimaging [5], subsurface exploration [6], and astronomical observations through turbulent atmospheres [7]. As such, the study of speckle has recently become of central importance in extracting information from—or transmitting it through—complex turbid media [8–14].

In a multiplicity of contexts, light may be confined to propagate on the sites of a discrete lattice, such as those defined by coupled photorefractive [15], semiconductor [16], or femtosecond laser written silica [17] waveguide arrays, random fiber cores [18], coupled optical resonators [19], or photonic crystal waveguides [20]. Whether classical [15–20] or quantum light [21–24] is utilized, propagation of an extended coherent field along a disordered photonic lattice produces *discrete speckle* on the lattice sites [Fig. 1(b)], in contrast to conventional continuous speckle. One feature arising from the interference between randomly scattered waves in an otherwise periodic potential is Anderson localization [25,26], which is manifested in the lack of diffusion of the wave function. Optics has enabled direct observation of so-called transverse localization [27] in coupled waveguide arrays on a transversely disordered lattice [15–18,28], among other realizations [29]. Usually in such experiments, only a single waveguide is excited and *spatially nonstationary* discrete speckle develops. The typical measure of localization in this scenario is the spatial width of the ensemble-averaged intensity distribution of transmitted light [28]. If instead the waveguides are illuminated by extended coherent light, a configuration that has not been thoroughly investigated heretofore [16,30], a discrete speckle pattern with *spatially invariant statistics* develops that apparently masks the localization signature.

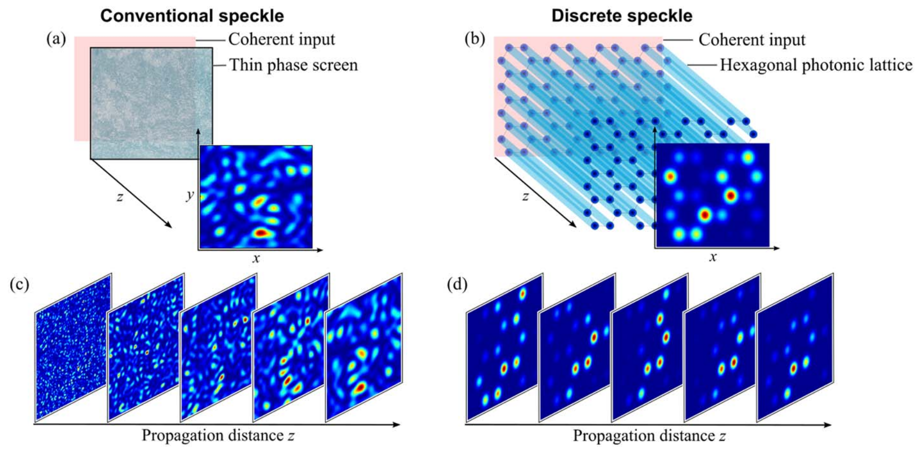

Fig. 1. Conventional speckle and discrete Anderson speckle. (a) A thin random phase screen ($\sigma_\phi = 4\pi$) illuminated with a uniform coherent beam produces conventional speckle. (b) Discrete Anderson speckle is produced from a highly disordered hexagonal (honeycomb) waveguide lattice with maximal off-diagonal disorder when illuminated with a uniform coherent beam. (c) The grain size of conventional speckle increases with propagation distance z, while that of discrete Anderson speckle does not as shown in (d).

In this work, we investigate numerically and analytically the statistical properties of discrete speckle in one- and two-dimensional (1D and 2D) disordered Anderson lattices upon extended illumination [Fig. 1(b)]. We show that the fingerprint of localization is embedded in the fluctuations of the emerging light and is thus revealed in the coherence function. We uncover a surprising phenomenon: the transverse coherence width associated with an extended coherent field is determined by the localization length resulting from a single-site excitation. Consequently, beyond a critical distance, the transverse speckle grain size "freezes" upon subsequent propagation along the lattice [Fig. 1(d)]. Furthermore, the axial coherence depth is independent of axial position, leading to a coherence "voxel" of fixed volume independent of position. We take these features collectively to define a new regime that we call "discrete Anderson speckle." Our findings are in contradistinction to the familiar characteristics of conventional speckle [31], wherein the transverse coherence length grows with the free-space propagation distance [Fig. 1(c)], as dictated by the van Cittert–Zernike theorem [32].

These findings have their foundation in the different beam propagation dynamics that distinguish discrete lattices from continuous media. Nevertheless, despite the distinctions between conventional and discrete Anderson speckle, both phenomena have a common feature: each system contains a single realization of a random function of the transverse coordinate. In conventional speckle, the randomness is confined to the thin screen while, in discrete Anderson speckle, it extends axially without change. Our results help elucidate the ultimate resolution limits of imaging through an Anderson lattice [18], introduce new strategies for engineering the spatial optical coherence of a beam of light [33], and indicate the potential for tuning higher-order field statistics beyond the Gaussian limits.

Previous investigations of electromagnetic-wave propagation through random media have studied the dimensionless conductance, which is proportional to the transmittance [34–36]. In such systems disorder, and hence localization, is primarily *axial* instead of transverse. In case of the 1D and 2D photonic systems examined here, the situation is quite distinct since the disorder is transverse and back-scattering is not allowed, so that the transmittance is always unity (in the absence of absorption) and the localization is observed in a plane transverse to the propagation axis.

2. DISCRETE OPTICAL LATTICE MODEL

Field propagation along a 1D lattice of parallel waveguides with evanescent nearest-neighbor-only coupling [Fig. 2] is given by the coupled equation [29]

$$i\frac{dE_x(z)}{dz} + \beta_x E_x + C_{x,x-1}E_{x-1} + C_{x,x+1}E_{x+1} = 0, \quad \textbf{(1)}$$

where $E_x(z)$ is the complex optical field in the xth waveguide ($x = -N, \ldots, N$) at axial position z, β_x is the propagation constant of waveguide x, and $C_{x,x+1}$ is the coupling coefficient between adjacent waveguides x and $x+1$. The evolution of the input field $E_i(x_i)$ to the output $E_o(x_o)$ at z may be written as $E_o(x_o) = \sum_{x_i} h(x_o, x_i)E_i(x_i)$, where $h(x_o, x_i)$ represents the system's impulse response function after propagating an axial distance z (see Supplement 1). The point spread function (PSF) $|h(x_o, x_i)|^2$ is the corresponding output intensity. This formulation may be readily extended to 2D lattices (Fig. 3).

A. Disorder Classes

We consider two classes of disorder. The first, *diagonal* disorder [25], is characterized by constant $C_{x,x+1} = \bar{C}$ and random β_x having a uniform probability distribution of mean $\bar{\beta}$ and half width $\Delta\beta$. The second class, *off-diagonal* disorder [37], is characterized by fixed $\beta_x = \bar{\beta}$ and random $C_{x,x+1}$ having a uniform probability distribution of mean $\bar{C}$ and half width ΔC. Both disorder classes exhibit similar behavior in our investigations; we thus report here results for off-diagonal disorder and relegate those for diagonal disorder to Supplement 1.

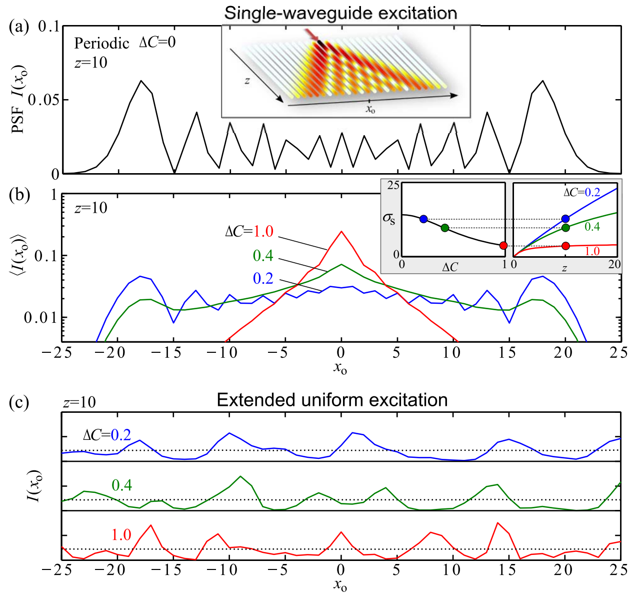

Fig. 2. Anderson localization and discrete speckle in 1D waveguide lattices. (a) PSF $I(x_o) = |h(x_o, 0)|^2$ at $z = 10$ for a 1D periodic array for single-waveguide excitation at $x_i = 0$. Inset is a schematic of the configuration. (b) Mean PSF $\langle I(x_o)\rangle = \langle |h(x_o, 0)|^2\rangle$ for disordered 1D arrays. Insets show the localization length σ_s as a function of ΔC (for fixed $z = 10$) and of z (for fixed values of ΔC). For the values of σ_s in the insets, 21 points for ΔC and 200 for z are chosen. (c) Realizations of discrete speckle at various disorder levels ($z = 10$) for extended uniform coherent input light. The dotted lines are ensemble averages. We use $N_t = 151$ throughout.

The findings of this study are presented in terms of dimensionless variables by writing the coupling coefficients in units of their average $\bar{C}$, and the distance z in units of the coupling length $\ell = 1/\bar{C}$. Throughout, ΔC ranges from 0 to 1. Lattice sizes are chosen large enough so that all the central results in this work are independent of lattice size $N_t = 2N + 1$. Further details are provided in Supplement 1.

3. DISCRETE ANDERSON SPECKLE: TRANSVERSE COHERENCE

A. Anderson Localization

To set the stage for examining transverse coherence of discrete speckle in Anderson lattices upon uniform illumination, we first describe briefly the results of single-waveguide excitation. When disorder is absent ($\Delta C = 0$), ballistic spread leads to an extended output state [Fig. 2(a)]. Progressively introducing disorder into the lattice results in a gradual transition to an exponentially localized state [Fig. 2(b)] manifested in the pronounced confinement of the mean PSF $\langle |h(x_o, 0)|^2\rangle$ around the excitation waveguide, where $\langle\cdot\rangle$ is the ensemble average. In general, similar behavior is observed in 2D lattices [Fig. 3(a)]. We define the localization length σ_s as the root-mean-square width of the mean PSF. As shown in Figs. 2(b) (inset) and 3(b), σ_s decreases monotonically with increasing ΔC at fixed distance z in 1D and 2D lattices. On the other hand, σ_s typically increases with z at fixed ΔC until it saturates, a signature of localization, which happens earlier for large ΔC [Fig. 2(b), inset]. For later reference, we note that for short propagation distances at intermediate disorder levels, features of both localized and ballistic states coexist.

B. Transverse Coherence

We now move on to our investigation of the global statistics of light in Anderson lattices by examining the case of coherent extended uniform illumination. For a 1D array, $E_i(x_i) = 1$ and the output field is $E_o(x_o) = \sum_{x_i} h(x_o, x_i)$, which is a random function of x_o in the case of a disordered lattice; a similar relation holds for 2D arrays. In the absence of disorder, the extended intensity distribution is invariant with respect to propagation [Fig. 3(c) for 2D]. Upon introducing disorder, this uniform distribution transitions into a granular intensity pattern $I(x_o) = \langle |E_o(x_o)|^2\rangle$ defined on the lattice sites, which we call discrete speckle. Examples of individual realizations for 1D and 2D lattices are shown in Figs. 2(c) and 3(c),

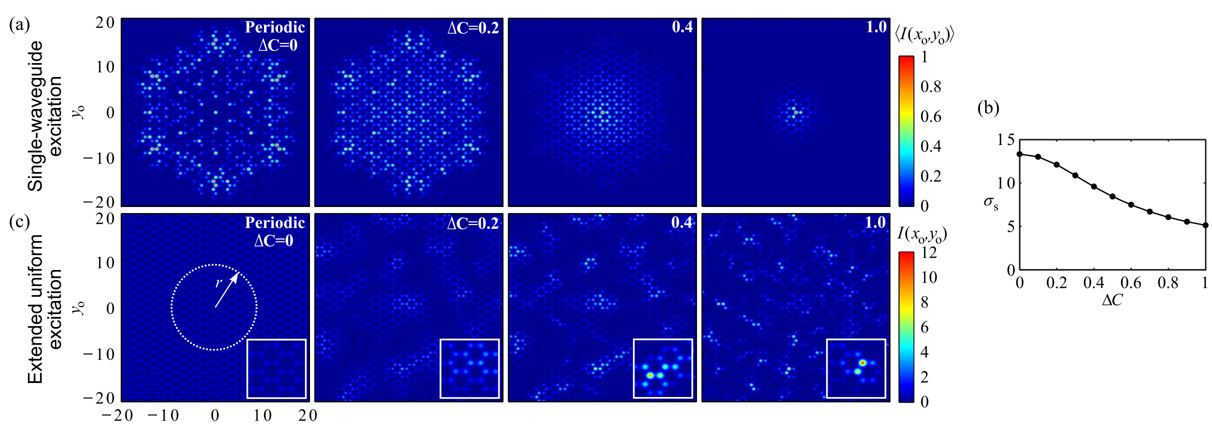

Fig. 3. Anderson localization and discrete speckle in 2D waveguide lattices. (a) Mean PSF $\langle I(x_o, y_o)\rangle = \langle |h(x_o, 0; y_o, 0)|^2\rangle$ for 2D hexagonal (honeycomb) arrays with increasing disorder (from left to right) at $z = 10$. For clarity, each panel is normalized separately and convolved with a Gaussian function of width 1.6 for better visualization. (b) Localization radius σ_s as a function of disorder level ΔC. For the values of σ_s shown, 11 points for ΔC are chosen. (c) Individual realizations of discrete speckle at various disorder levels corresponding to the panels in (a) upon extended uniform coherent illumination. Note that the speckle grain size decreases with increasing disorder. Insets are magnified by a factor of 2. Speckle contrasts are 0, 0.76, 1.22, and 1.24 from left to right. We use $N_t \times N_t = 101 \times 101$ throughout.

respectively. Several characteristics are immediately apparent in these results. First, with increasing disorder, the grain size–which is related to the transverse spatial coherence width–decreases. On the other hand, the speckle contrast c, defined as the ratio of the standard deviation in the speckle intensity σ_I to its mean intensity $\bar{I}$, $c = \sigma_I/\bar{I}$, increases with disorder. These observations are telltale signs of a decrease in the transverse coherence width with increasing disorder. Indeed, these characteristics are shared with conventional speckle [31].

Despite the spatially varying intensity distribution $|E_o(x_o)|^2$ in the individual realizations for extended input, the statistical homogeneity of this discrete speckle is clear in the uniform distribution obtained upon averaging multiple realizations $\langle |E_o(x_o)|^2 \rangle$ [the dotted lines in Fig. 2(c)]. The coherence function at a pair of positions x_o and $x_o + x$ in 1D is therefore a function of only the separation x,

$$G^{(1)}(x_o, x_o + x) = G^{(1)}(0, x) = \langle E_o^*(0) E_o(x) \rangle = \sum_{x', x''} \langle h(0, x') h(x, x'') \rangle. \quad \textbf{(2)}$$

Its normalized version is the complex degree of coherence $g^{(1)}(x) = G^{(1)}(0,x)/\sqrt{G^{(1)}(0,0)G^{(1)}(x,x)}$, with $0 \le |g^{(1)}(x)| \le 1$. In 2D discrete speckle, we similarly write the complex degree of coherence $g^{(1)}(r)$ as a function of the radial separation distance r shown in Fig. 3(c). For later reference (see Section 5), we note that transverse spatial invariance results in the double summation in Eq. (2) separating over the two impulse response functions, such that $G^{(1)}(0, x) = \langle \eta \sum_{x''} h(x, x'') \rangle$, where $\eta = \sum_{x'} h^*(0, x')$ is a zero-mean, complex random variable.

We have carried out an extensive computational exploration of the coherence properties of light propagating in Anderson lattices. Figures 4(a) and 5(a) depict the magnitudes of $g^{(1)}(x)$ and $g^{(1)}(r)$ for 1D and 2D lattices, respectively, revealing a nonzero pedestal $|g^{(1)}(\infty)|$ riding on which is a finite-width distribution. This pedestal $|g^{(1)}(\infty)|$ signifies the survival of long-range transverse order; that is, some level of transverse correlation is maintained regardless of the separation between the pair of waveguides. Indeed, $|g^{(1)}(\infty)|$ decreases monotonically with ΔC until it vanishes altogether at a threshold ΔC value [Fig. 4(b) for 1D and Fig. 5(b) for 2D].

It is useful at this point to compare the coherence of discrete speckle just described to that of conventional speckle produced in the arrangement shown in Fig. 1(a). The random component of the screen phase ϕ is typically a Gaussian process with zero mean, variance σ_ϕ^2, and spatially invariant transverse correlation of width x_c, which we take as a transverse unit length in analogy to the unit separation between the waveguides on a lattice. During propagation along z, the field passes through two regimes. In the first regime, where $z < 2N_c x_c^2/\lambda$ (N_c is the size of the illuminating beam in units of x_c and λ is the wavelength), the coherence properties do not change with z. Interestingly, the coherence function $g^{(1)}(x)$ for conventional

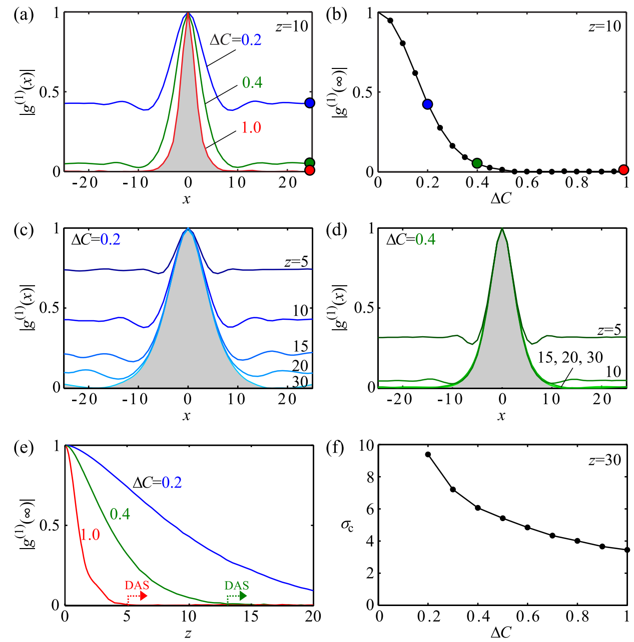

Fig. 4. Transverse coherence for 1D discrete Anderson speckle. (a) Magnitude of $g^{(1)}(x)$ for 1D arrays for various disorder levels ΔC at propagation distance $z = 10$. (b) Long-range-order coherence pedestal $|g^{(1)}(\infty)|$ as a function of ΔC at $z = 10$. The circles in (b) correspond to the same values of ΔC in (a). Magnitude of $g^{(1)}(x)$ at various z for (c) $\Delta C = 0.2$ and (d) $\Delta C = 0.4$. The pedestal decreases with z and $g^{(1)}(x)$ becomes stationary with respect to further propagation. (e) $|g^{(1)}(\infty)|$ as a function of z at various ΔC. (f) Transverse coherence width σ_c as a function of ΔC at $z = 30$. All areas shaded in gray, and also the dashed arrows, indicate the onset of the discrete Anderson speckle (DAS) regime.

speckle contains a pedestal associated with the specular component of the field when the thin phase screen has small σ_ϕ^2 [31], in analogy to the pedestal resulting from ballistic propagation in its discrete counterpart for small ΔC [Figs. 4(a) and 5(a)]. In conventional speckle, the pedestal height drops gradually with increased σ_ϕ^2 for fixed z [similar to the behavior of $|g^{(1)}(\infty)|$ with ΔC in Figs. 4(b) and 5(b)], and gradually vanishes as the field leaves this regime, i.e., $z > 2N_c x_c^2/\lambda$. In the far field, $g^{(1)}(x)$ becomes the Fourier transform of the illumination spot and the grain size increases continuously with z in accordance with the van Cittert–Zernike theorem [Fig. 1(c)].

A distinction between near and far field may be similarly made for discrete speckle based on the disappearance of the pedestal $g^{(1)}(\infty)$. For small distances, $g^{(1)}(\infty)$ is nonzero and the discrete speckle undergoes dynamical changes upon propagation, as shown in Figs. 4(c) and 4(d). However, for a given disorder level ΔC, the pedestal vanishes after some distance $z > \frac{5}{\Delta C}$ [Fig. 4(e)] that we determined empirically–which we take as an indication that the far field has been reached ($z > \frac{10}{\Delta \beta}$ for arrays with diagonal disorder). Beyond this axial distance, $g^{(1)}(x)$ is stationary and the grain size freezes. This observation is a glaring departure from conventional speckle, where grain size increases upon propagation in the far field. We call discrete speckle in this regime discrete

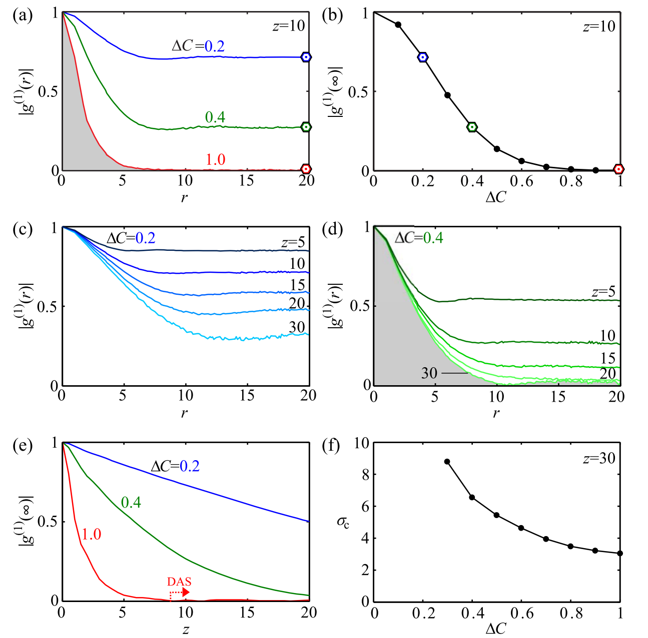

Fig. 5. Transverse coherence for 2D discrete Anderson speckle. (a) Magnitude of $g^{(1)}(r)$ for 2D arrays for various disorder levels ΔC at propagation distance $z = 10$. (b) Long-range-order coherence pedestal $|g^{(1)}(\infty)|$ as a function of ΔC at $z = 10$. The hexagons in (b) correspond to the same values of ΔC in (a). Magnitude of $g^{(1)}(r)$ at various z for (c) $\Delta C = 0.2$ and (d) $\Delta C = 0.4$. The pedestal height decreases with z, and $g^{(1)}(x)$ becomes stationary with respect to further propagation. (e) $|g^{(1)}(\infty)|$ as a function of z at various ΔC. (f) Transverse coherence width σ_c as a function of ΔC at $z = 30$. All areas shaded in gray, and also the dashed arrows, indicate the onset of the DAS regime.

Anderson speckle, since we will show later that the transverse coherence width σ_c here is dictated by the localization length σ_s. We define the coherence width σ_c (or grain size) as the full width at half-maximum (FWHM) of the steady state $|g^{(1)}(x)|$ [that is, in the far field where the pedestal $g^{(1)}(\infty)$ disappears]. We find that σ_c decreases monotonically with ΔC, as shown in Fig. 4(f). In the near field, the pedestal in effect reduces the speckle grain size by screening the steady-state $|g^{(1)}(x)|$. Freezing of the coherence function with propagation takes place slower in 2D (Fig. 5).

To uncover the physics underlying this disorder-induced freezing of the grain size in the discrete Anderson regime, we compare σ_c for uniform illumination to the localization length σ_s resulting from a single-waveguide excitation. For this comparison, we redefine σ_s as the FWHM of the mean PSF. We find that these two very different quantities are in fact linearly proportional $\sigma_c \approx 1.3\sigma_s$ (Fig. 6). This may be understood by noting that in the presence of disorder, the PSF is a random function with finite average width [17,21,22]. Light emerging from waveguides separated by a distance greater than the PSF width are likely to have passed through nonoverlapping paths of the random array, and should therefore be uncorrelated. We will present below a general analytical argument that establishes the relationship between σ_c for extended illumination to σ_s for a single-waveguide excitation.

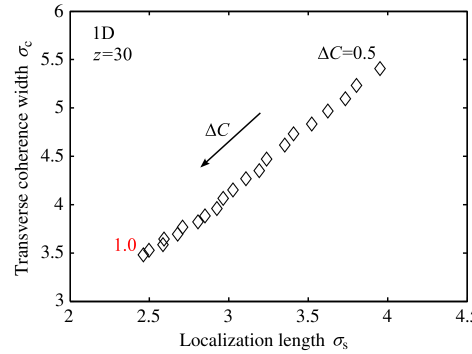

Fig. 6. Correlation between transverse coherence and localization in the discrete Anderson speckle regime. Correlation between σ_s and σ_c with varying disorder level at $z = 30$. Here, σ_s is the FWHM of the mean PSF and σ_c is the FWHM of the degree of transverse coherence $|g^{(1)}(x)|$. The axial distance $z = 30$ is selected such that the discrete Anderson speckle regime (where $|g^{(1)}(\infty)| \approx 0$) has been reached for all disorder levels from $\Delta C = 0.5$ to 1.

4. DISCRETE ANDERSON LOCALIZATION: AXIAL COHERENCE

Further insight may be drawn from a detailed examination of the axial coherence propagation dynamics. We plot $I(x_o; z) = |E(x_o; z)|^2$ for three realizations at $\Delta C = 0.2$, 0.4, 1.0 in Fig. 7(a). The longitudinal freezing of the transverse discrete speckle is evident for all three cases in the far field, resulting in axial filamentation of the intensity distribution corresponding to the nonoverlapping, uncorrelated paths along the disordered lattice mentioned previously. Evaluation of the axial coherence

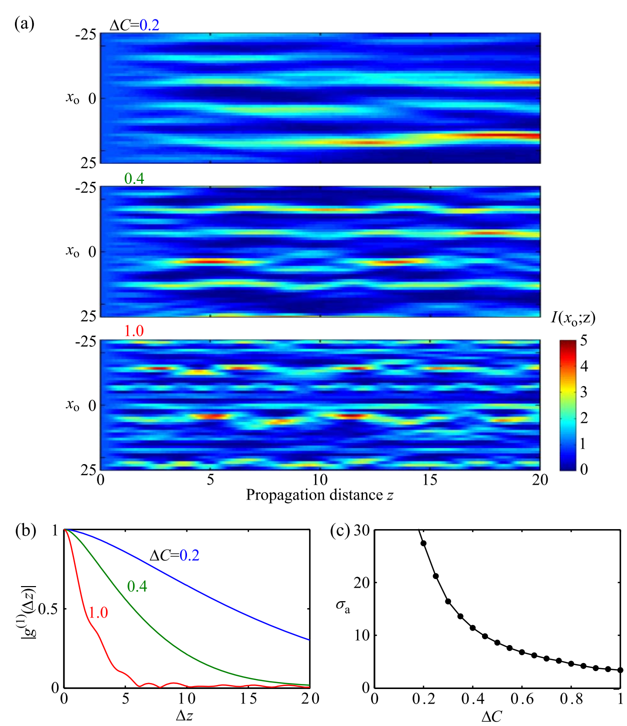

Fig. 7. Axial coherence in 1D discrete Anderson speckle. (a) Axial evolution of the intensity in individual realizations of 1D lattices with different ΔC. (b) Amplitude of the axial coherence function $|g^{(1)}(\Delta z)|$. (c) Axial coherence depth σ_a for different ΔC.

function $G^{(1)}(z, \Delta z) = \Sigma_{x_o} \langle E^*(x_o; z) E(x_o; z + \Delta z) \rangle$ reveals that it is in fact independent of z altogether. The normalized axial degree of coherence $|g^{(1)}(\Delta z)|$ decays with Δz at a rate proportional to the disorder level [Fig. 7(b)], so that its FWHM or axial coherence depth σ_a drops with disorder [Fig. 7(c)]. This behavior is stationary along z. Finally, a unique aspect of the features described in this section is that they are evident in individual realizations, unlike observations of Anderson localization that necessitate ensemble averaging.

We have found that the transverse coherence width σ_c reaches a steady state in the discrete Anderson speckle regime, and the statistical homogeneity renders it independent of transverse position x. Furthermore, the axial coherence depth σ_a for a fixed disorder level is independent of axial position z (and is primarily due to dephasing; see Figs. S3–S5 in Supplement 1). By combining these findings concerning transverse and axial coherence in disordered lattices, we conclude that a coherence voxel of fixed volume exists everywhere along the lattice in the discrete Anderson speckle regime. The volume of this coherence voxel depends solely on the disorder level ΔC. This behavior is once again a dramatic departure from that of conventional speckle where the transverse coherence growth in the far field is dictated by the van Citter–Zernike theorem, and this growth in transverse coherence length is accompanied by a reduction in the axial coherence length.

5. ANALYTICAL MODEL

We have shown numerically that the fingerprint of localization exists in the fluctuations of the discrete speckle emerging from Anderson lattices for an extended coherent input. It may be initially surprising that a link exists between the localization length (typically associated with a point excitation and averaging over output intensity) and the transverse coherence width (associated with an extended input and averaging over field products for pairs of waveguides); see Fig. 6. Our goal here is to link the extended-illumination scheme that has been our focus [Fig. 1(b)] with the more usual single-waveguide excitation strategy [Figs. 2(a)–2(b)]. To elucidate this link, we adapt to our setting a conceptual scheme from quantum optics known as Klyshko's advanced-wave picture [38,39], which is also of use to classical fields. This scheme allows for the identification of correlation functions of an extended field traversing an optical system with the field or intensity of a double-pass configuration (backward then forward) of a point source through the same system.

We start by depicting in Fig. 8(a) the 1D scenario we have investigated in this work, whereupon an extended coherent

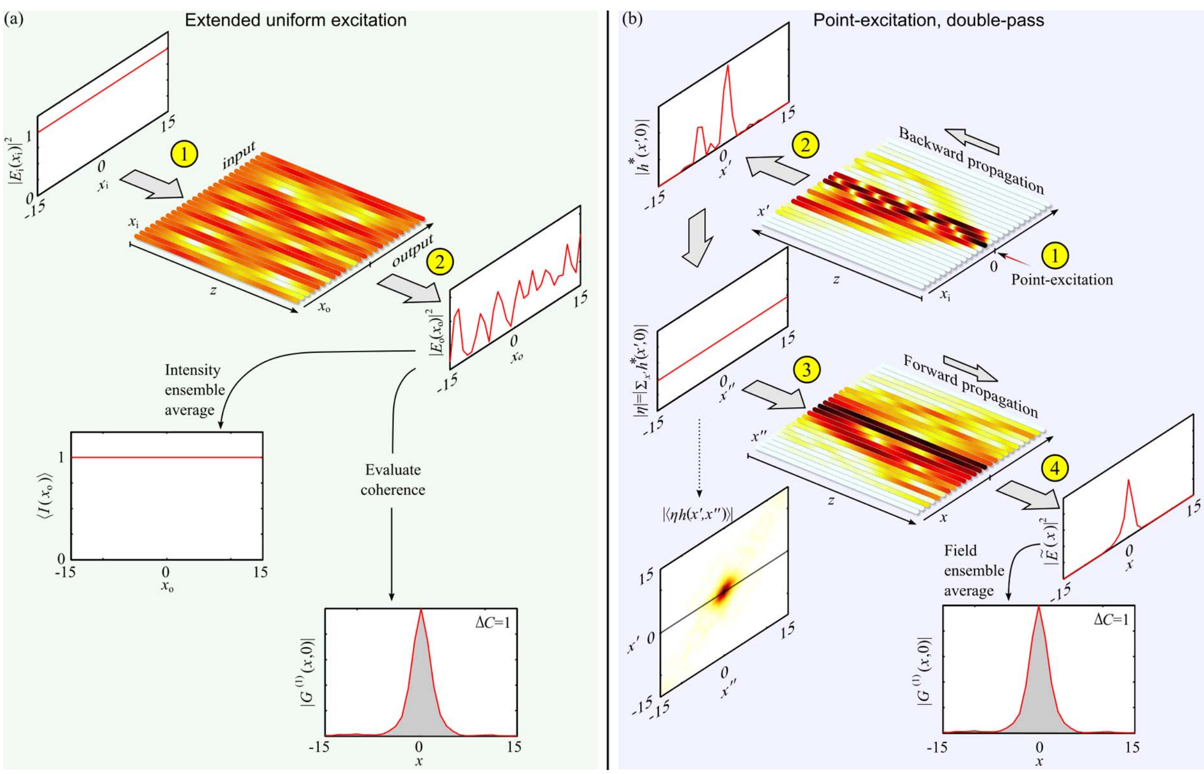

Fig. 8. Heuristic model linking the transverse coherence width to the localization length in an Anderson lattice. (a) Schematic for extended uniform excitation $E_i(x_i) = 1$ in an array of waveguides resulting in an output field $E_o(x_o)$ having a narrow transverse coherence function with no pedestal. Here, $\Delta C = 1$ and z is taken such that we are in the discrete Anderson speckle regime. Ensemble averaging of the output intensity $\langle |I(x_o)|^2 \rangle$ yields a constant. (b) Representation of Klyshko's advanced-wave picture in which an unfolded cascade of systems is excited at a single point ($x_i = 0$) and whose output may be put in correspondence with that of the extended illumination configuration in (a). The field propagates backward through the disordered lattice [as a result of the conjugation in Eq. (3)], and a spatial average of the output field $\eta = \Sigma_{x'} h^*(0, x')$ is evaluated. An extended uniform field with random complex amplitude η propagates forward through the same realization of the lattice to produce an output field $\tilde{E}(x)$ whose ensemble average $\langle \tilde{E}(x) \rangle$ corresponds to the coherence function in (a). We also plot the function $\langle \eta h(x', x'') \rangle$ for reference. $\Delta C = 1$ and ensemble size is 10^4 in (a)–(b).

field traverses a random lattice ($\Delta C = 1$). Averaging the output intensity $|E_o(x_o)|^2$ over multiple realizations yields a constant distribution with no localization signature [Fig. 2(c)]. Nevertheless, computing the spatially stationary coherence function $G^{(1)}(0, x)$ by averaging over products of fields from pairs of waveguides separated by x yields a localized function (independently of x_o) of width σ_c. Referring to Eq. (2), we write $G^{(1)}(0, x)$ as

$$G^{(1)}(0, x) = \langle \overbrace{\sum_{x''} h(x, x'')}^{\text{forward}} \underbrace{\sum_{x'}}_{\text{averaging}} \overbrace{h^*(0, x')}^{\text{backward}} \rangle. \quad (3)$$

This equation can be interpreted in light of the Klyshko advanced-wave picture as a cascade of the three steps illustrated in Fig. 8(b). First, a point excitation at $x_i = 0$ propagates backward through the system h to the x' plane, as dictated by the conjugation operation. Second, the output field from this backward propagation is spatially averaged over x' to yield the complex random variable $\eta = \Sigma_{x'} h^*(0, x')$, which is then equally distributed over points x'' in the input plane for a second pass forward through the same realization of the system h. Third, the uniform extended field of amplitude η propagates forward through h to produce an output random field $\widetilde{E}(x) = \eta \Sigma_{x''} h(x, x'')$. Ensemble averaging results in $\langle \widetilde{E}(x) \rangle = G^{(1)}(0, x)$ per Eqs. (2) and (3).

Let us examine the third step in this cascade, the forward pass. Each waveguide at position x'' is fed with a noisy field having complex random amplitude η with zero mean. The ensemble average of the output field in the x plane contributed by each waveguide is $\langle \eta h(x, x'') \rangle$. While the ensemble average of $\langle \eta \rangle$ and $\langle h(x, x'') \rangle$ (for high disorder levels) is each zero, the average of their product need not be so since both random variables are generated by the same realization of the disordered lattice. Indeed, since η is generated by the random lattice environment in the vicinity of $x = 0$ in the Anderson localization limit, then it correlates only with h in the same vicinity, while remaining uncorrelated $\langle \eta h(x, x'') \rangle \sim 0$ when h is evaluated away from the origin, as shown in Fig. 8(b). Consequently, only a few waveguides in the vicinity of $x'' = 0$ contribute to the forward pass. Since h produces a localized output for a point excitation, the few-waveguide excitation here results in a slightly broader localized spot whose width is σ_c [resulting from the convolution of the impulse response function with the width of the distribution in Fig. 8(b)]. We have thus established on these grounds that σ_c is intimately linked with the localization length σ_s, but is expected to be slightly larger, as was shown numerically in Fig. 6.

We next proceed to an analytical model of discrete Anderson speckle based on modal analysis. Using the eigenmodes of the lattice coupling matrix, we justify (1) the freezing of the transverse coherence width σ_c (and hence the speckle grain size) once the discrete Anderson speckle regime is reached, and (2) the independence of the axial coherence depth σ_a from the axial position z.

A. Origin of the Freezing of the Transverse Coherence Width

We analyze the propagation of the field along an Anderson lattice in terms of the eigenmodes and eigenvalues of the Hermitian coupling matrix $\hat{\mathbf{H}}$ that is defined by the equation of dynamics in Eq. (1) by writing

$$i\frac{d\mathbf{E}(z)}{dz} + \hat{\mathbf{H}}\mathbf{E} = 0, \quad (4)$$

where $\mathbf{E}$ is a vector of length $2N + 1$ containing the field amplitudes in the waveguides, and $\hat{\mathbf{H}}$ is a real symmetric (and hence Hermitian) matrix with the wave numbers along the diagonal and coupling coefficients off the diagonal. If the eigenmodes and eigenvalues of $\hat{\mathbf{H}}$ are $\phi_n(x)$ and b_n, respectively, then since $h = e^{i\hat{\mathbf{H}}z}$, the eigenvalue problem is defined for the impulse response function as

$$\sum_{x'} h(x, x'; z)\phi_n(x') = e^{ib_n z}\phi_n(x), \quad (5)$$

such that the impulse response function may be expressed as

$$h(x_o, x_i; z) = \sum_n e^{ib_n z}\phi_n(x_o)\phi_n(x_i). \quad (6)$$

We have made use of the fact that the eigenmodes are real since $\hat{\mathbf{H}}$ is real and symmetric. Using this definition, we recast the joint transverse-axial coherence function in terms of $\phi_n(x)$ and b_n,

$$\begin{aligned} &G^{(1)}(0, x; z, z + \Delta z) \\ &= \sum_{x', x''} \langle h^*(0, x'; z) h(x, x''; z + \Delta z) \rangle \\ &= \sum_{x', x''} \sum_{n,m} \langle \phi_n(0)\phi_n(x')\phi_m(x)\phi_m(x'') e^{i(b_n - b_m)z} e^{-ib_m \Delta z} \rangle. \quad (7) \end{aligned}$$

The freezing of the speckle grain size in the discrete Anderson speckle regime is realized at large propagation distances z when the condition $\mathrm{Std}\{b_n\} z \gtrsim 2\pi$ is satisfied; here, $\mathrm{Std}\{\cdot\}$ is the standard deviation. We expect that $\mathrm{Std}\{b_n\}$ is proportional to ΔC, such that the distance z that satisfies this condition is inversely proportional to ΔC. In the case of off-diagonal disorder, which we have considered here, the eigenvalue b_0 is excluded from this condition since it remains deterministic with value 0 [40]. This exclusion is not required in the case of diagonal disorder which is described in Supplement 1. We have found numerically that this limit in lattices with off-diagonal disorder is attained when $z > \frac{5}{\Delta C}$, which we have taken to define the discrete Anderson speckle regime.

When the condition $\mathrm{Std}\{b_n\} z \gtrsim 2\pi$ is met, the difference $b_n - b_m$ when $n \neq m$ has the same order of magnitude as this standard deviation, but is equal to zero when $n = m$, therefore implying that upon ensemble averaging, the impact of the exponential term in Eq. (7) is $e^{i(b_n - b_m)z} \to \delta_{n,m}$. Thus, setting $\Delta z = 0$ in the axial regime where $z > \frac{5}{\Delta C}$, Eq. (7) reduces to

$$G^{(1)}(0,x;z,z) = \sum_{x',x''}\sum_{n}\langle\phi_n(0)\phi_n(x)\phi_n(x')\phi_n(x'')\rangle. \quad \textbf{(8)}$$

This equation implies that, in the discrete Anderson speckle regime, the transverse coherence is a function of the separation x but not the axial distance z, as demonstrated numerically in Fig. 4.

B. Independence of Axial Coherence Depth from Axial Position

In considering the axial coherence along the lattice, we make use of the transverse stationarity of the lattice and consider a single lattice site x in Eq. (7), whereupon the axial coherence function is

$$G^{(1)}(x,x;z,z+\Delta z) = \sum_{x',x''}\sum_{n,m}\langle\phi_n(x)\phi_n(x')\phi_m(x)\phi_m(x'')e^{i(b_n-b_m)z}e^{-ib_m\Delta z}\rangle. \quad \textbf{(9)}$$

By taking a spatial average over x, we obtain a simplified relation

$$\sum_x G^{(1)}(x,x;z,z+\Delta z) = \sum_{x',x''}\sum_{n}\langle\phi_n(x')\phi_n(x'')e^{-ib_n\Delta z}\rangle, \quad \textbf{(10)}$$

in which we used $\sum_x\phi_n(x)\phi_m(x) = \delta_{n,m}$. Consequently, the axial coherence function averaged over the transverse coordinate is altogether independent from z. However, since $G^{(1)}(x,x;z,z+\Delta z)$ is stationary in x, its statistical properties are the same as those of $\sum_x G^{(1)}(x,x;z,z+\Delta z)$. Therefore, the axial coherence function is independent of z, and as a result its width σ_a is also independent of z and relies only on Δz, as demonstrated numerically in Fig. 7.

6. CONCLUSION

We have investigated the evolution of a set of mutually coherent waves traveling through 1D and 2D disordered lattices of coupled waveguides. The emerging wave forms discrete speckle that is statistically homogeneous with random intensity distribution on the lattice sites. The disordered lattice structure that results in Anderson localization when a single waveguide is excited exhibits, in the case of an extended excitation, a complete freezing of the discrete speckle grain size after reaching a steady state, unlike the usual growth observed in conventional speckle–a regime we refer to as discrete Anderson speckle. Moreover, axial and transverse coherence are independent of position, resulting in a coherence voxel of fixed volume independent of its transverse and axial position on the lattice. These results are applicable to a broad host of photonic systems in which disorder may impact coupling between discrete elements [15–23]. While we have studied second-order field correlations on a discrete lattice, the new behavior reported here signposts important vistas to be investigated in the context of higher-order correlations and photon statistics [41].

Finally, the correspondence between the propagation of light and that of a quantum particle on discrete lattices [29] has led recently to fruitful exchanges between optical and condensed matter physics [42–48]. Our result, therefore, points to new regimes that may be investigated in other physical systems, ranging from Bose–Einstein condensates [49] to acoustic lattices [50], where Anderson localization takes place owing to interference of random waves.

ACKNOWLEDGMENT

The authors thank the Stokes Advanced Research Computing Center at the University of Central Florida for access to the high-performance computing cluster.

See Supplement 1 for supporting content.

REFERENCES

1. J. D. Rigden and E. I. Gordon, "The granularity of scattered optical maser light," Proc. IRE **50**, 2367 (1962).
2. B. M. Oliver, "Sparkling spots and random diffraction," Proc. IEEE **51**, 220–221 (1963).
3. J. A. Ratcliffe and J. L. Pawsey, "A study of the intensity variations of downcoming wireless waves," Math. Proc. Cambridge Philos. Soc. **29**, 301–318 (1933).
4. H. G. Booker, J. A. Ratcliffe, and D. H. Shinn, "Diffraction from an irregular screen with applications to ionospheric problems," Phil. Trans. R. Soc. A **242**, 579–607 (1950).
5. J. Bertolotti, E. G. van Putten, C. Blum, A. Lagendijk, W. L. Vos, and A. P. Mosk, "Non-invasive imaging through opaque scattering layers," Nature **491**, 232–234 (2012).
6. B. E. A. Saleh, *Introduction to Subsurface Imaging* (Cambridge University, 2011).
7. A. Labeyrie, "Attainment of diffraction limited resolution in large telescopes by Fourier analysing speckle patterns in star images," Astron. Astrophys. **6**, 85–87 (1970).
8. A. P. Mosk, A. Lagendijk, G. Lerosey, and M. Fink, "Controlling waves in space and time for imaging and focusing in complex media," Nat. Photonics **6**, 283–292 (2012).
9. B. Redding, M. A. Choma, and H. Cao, "Speckle-free laser imaging using random laser illumination," Nat. Photonics **6**, 355–359 (2012).
10. O. Katz, E. Small, and Y. Silberberg, "Looking around corners and through thin turbid layers in real time with scattered incoherent light," Nat. Photonics **6**, 549–553 (2012).
11. O. Katz, P. Heidmann, M. Fink, and S. Gigan, "Non-invasive single-shot imaging through scattering layers and around corners via speckle correlations," Nat. Photonics **8**, 784–790 (2014).
12. T. E. Matthews, M. Medina, J. R. Maher, H. Levinson, W. J. Brown, and A. Wax, "Deep tissue imaging using spectroscopic analysis of multiply scattered light," Optica **1**, 105–111 (2014).
13. O. Katz, E. Small, Y. Guan, and Y. Silberberg, "Noninvasive nonlinear focusing and imaging through strongly scattering turbid layers," Optica **1**, 170–174 (2014).
14. E. H. Zhou, H. Ruan, C. Yang, and B. Judkewitz, "Focusing on moving targets through scattering samples," Optica **1**, 227–232 (2014).
15. T. Schwartz, G. Bartal, S. Fishman, and M. Segev, "Transport and Anderson localization in disordered two-dimensional photonic lattices," Nature **446**, 52–55 (2007).
16. Y. Lahini, A. Avidan, F. Pozzi, M. Sorel, R. Morandotti, D. N. Christodoulides, and Y. Silberberg, "Anderson localization and nonlinearity in one-dimensional disordered photonic lattices," Phys. Rev. Lett. **100**, 013906 (2008).
17. L. Martin, G. Di Giuseppe, A. Perez-Leija, R. Keil, F. Dreisow, M. Heinrich, S. Nolte, A. Szameit, A. F. Abouraddy, D. N. Christodoulides, and B. E. A. Saleh, "Anderson localization in optical wave-

guide arrays with off-diagonal coupling disorder," Opt. Express **19**, 13636–13646 (2011).
18. S. Karbasi, R. J. Frazier, K. W. Koch, T. Hawkins, J. Ballato, and A. Mafi, "Image transport through a disordered optical fibre mediated by transverse Anderson localization," Nat. Commun. **5**, 3362 (2014).
19. S. Mookherjea, J. S. Park, S.-H. Yang, and P. R. Bandaru, "Localization in silicon nanophotonic slow-light waveguides," Nat. Photonics **2**, 90–93 (2008).
20. J. Topolancik, B. Ilic, and F. Vollmer, "Experimental observation of strong photon localization in disordered photonic crystal waveguides," Phys. Rev. Lett. **99**, 253901 (2007).
21. A. F. Abouraddy, G. Di Giuseppe, D. N. Christodoulides, and B. E. A. Saleh, "Anderson localization and colocalization of spatially entangled photons," Phys. Rev. A **86**, 040302 (2012).
22. G. Di Giuseppe, L. Martin, A. Perez-Leija, R. Keil, F. Dreisow, S. Nolte, A. Szameit, A. F. Abouraddy, D. N. Christodoulides, and B. E. A. Saleh, "Einstein-Podolsky-Rosen spatial entanglement in ordered and Anderson photonic lattices," Phys. Rev. Lett. **110**, 150503 (2013).
23. A. Crespi, R. Osellame, R. Ramponi, V. Giovannetti, R. Fazio, L. Sansoni, F. De Nicola, F. Sciarrino, and P. Mataloni, "Anderson localization of entangled photons in an integrated quantum walk," Nat. Photonics **7**, 322–328 (2013).
24. J. Svozilík, J. Peřina, and J. P. Torres, "Measurement-based tailoring of Anderson localization of partially coherent light," Phys. Rev. A **89**, 053808 (2014).
25. P. W. Anderson, "Absence of diffusion in certain random lattices," Phys. Rev. **109**, 1492–1505 (1958).
26. A. Lagendijk, B. van Tiggelen, and D. S. Wiersma, "Fifty years of Anderson localization," Phys. Today **62**(8), 24–29 (2009).
27. H. De Raedt, A. Lagendijk, and P. de Vries, "Transverse localization of light," Phys. Rev. Lett. **62**, 47–50 (1989).
28. M. Segev, Y. Silberberg, and D. N. Christodoulides, "Anderson localization of light," Nat. Photonics **7**, 197–204 (2013).
29. D. N. Christodoulides, F. Lederer, and Y. Silberberg, "Discretizing light behaviour in linear and nonlinear waveguide lattices," Nature **424**, 817–823 (2003).
30. D. Čapeta, J. Radić, A. Szameit, M. Segev, and H. Buljan, "Anderson localization of partially incoherent light," Phys. Rev. A **84**, 011801 (2011).
31. J. W. Goodman, *Speckle Phenomena in Optics: Theory and Applications* (Roberts & Company, 2007).
32. J. W. Goodman, *Statistical Optics* (Wiley, 2000).
33. B. Redding, M. A. Choma, and H. Cao, "Spatial coherence of random laser emission," Opt. Lett. **36**, 3404–3406 (2011).
34. Y. Imry and R. Landauer, "Conductance viewed as transmission," Rev. Mod. Phys. **71**, S306–S312 (1999).
35. A. A. Chabanov, M. Stoytchev, and A. Z. Genack, "Statistical signatures of photon localization," Nature **404**, 850–853 (2000).
36. J. Wang and A. Z. Genack, "Transport through modes in random media," Nature **471**, 345–348 (2011).
37. C. M. Soukoulis and E. N. Economou, "Off-diagonal disorder in one-dimensional systems," Phys. Rev. B **24**, 5698–5702 (1981).
38. D. V. Strekalov, A. V. Sergienko, D. N. Klyshko, and Y. H. Shih, "Observation of two-photon "ghost" interference and diffraction," Phys. Rev. Lett. **74**, 3600–3603 (1995).
39. D. N. Klyshko, "Quantum optics: quantum, classical, and metaphysical aspects," Phys. Uspekhi **37**, 1097–1123 (1994).
40. S. N. Evangelou and D. E. Katsanos, "Spectral statistics in chiral-orthogonal disordered systems," J. Phys. A **36**, 3237–3254 (2003).
41. Y. Lahini, Y. Bromberg, Y. Shechtman, A. Szameit, D. N. Christodoulides, R. Morandotti, and Y. Silberberg, "Hanbury Brown and Twiss correlations of Anderson localized waves," Phys. Rev. A **84**, 041806 (2011).
42. R. Morandotti, U. Peschel, J. S. Aitchison, H. S. Eisenberg, and Y. Silberberg, "Experimental observation of linear and nonlinear optical Bloch oscillations," Phys. Rev. Lett. **83**, 4756–4759 (1999).
43. F. Lederer, G. I. Stegeman, D. N. Christodoulides, G. Assanto, M. Segev, and Y. Silberberg, "Discrete solitons in optics," Phys. Rep. **463**, 1–126 (2008).
44. R. Iwanow, D. A. May-Arrioja, D. N. Christodoulides, G. I. Stegeman, Y. Min, and W. Sohler, "Discrete Talbot effect in waveguide arrays," Phys. Rev. Lett. **95**, 053902 (2005).
45. A. Peruzzo, M. Lobino, J. C. F. Matthews, N. Matsuda, A. Politi, K. Poulios, X.-Q. Zhou, Y. Lahini, N. Ismail, K. Wörhoff, Y. Bromberg, Y. Silberberg, M. G. Thompson, and J. L. OBrien, "Quantum walks of correlated photons," Science **329**, 1500–1503 (2010).
46. K. Shandarova, C. E. Rüter, D. Kip, K. G. Makris, D. N. Christodoulides, O. Peleg, and M. Segev, "Experimental observation of Rabi oscillations in photonic lattices," Phys. Rev. Lett. **102**, 123905 (2009).
47. M. C. Rechtsman, J. M. Zeuner, Y. Plotnik, Y. Lumer, D. Podolsky, F. Dreisow, S. Nolte, M. Segev, and A. Szameit, "Photonic Floquet topological insulators," Nature **496**, 196–200 (2013).
48. M. C. Rechtsman, Y. Plotnik, J. M. Zeuner, D. Song, Z. Chen, A. Szameit, and M. Segev, "Topological creation and destruction of edge states in photonic graphene," Phys. Rev. Lett. **111**, 103901 (2013).
49. J. Billy, V. Josse, Z. Zuo, A. Bernard, B. Hambrecht, P. Lugan, D. Clément, L. Sanchez-Palencia, P. Bouyer, and A. Aspect, "Direct observation of Anderson localization of matter waves in a controlled disorder," Nature **453**, 891–894 (2008).
50. H. Hu, A. Strybulevych, J. H. Page, S. E. Skipetrov, and B. A. van Tiggelen, "Localization of ultrasound in a three-dimensional elastic network," Nat. Phys. **4**, 945–948 (2008).